J Appl Electrochem (2014) 44:209–214
DOI 10.1007/s10800-013-0632-4

SHORT COMMUNICATION

A different method for producing a flexible $LiMn_2O_4$/MWCNT composite electrode for lithium ion batteries

Tugrul Cetinkaya · Ahsen Akbulut · Mehmet O. Guler · Hatem Akbulut

Received: 1 August 2013 / Accepted: 3 October 2013 / Published online: 13 October 2013

Abstract A flexible lithium manganese oxide ($LiMn_2O_4$)/multi-wall carbon nanotube (MWCNT) composite electrode was produced by casting a slurry-containing powdered $LiMn_2O_4$ on a previously prepared MWCNT paper. The structure of this new $LiMn_2O_4$/MWCNT composite electrode was characterized using scanning electron microscopy and X-ray diffraction patterns. Furthermore, the surfaces of these electrodes were coated with gold–palladium alloy using an RF magnetron sputtering technique to prevent Mn dissolution. To investigate the electrochemical performance of this flexible $LiMn_2O_4$/MWCNT composite electrode, a bare-$LiMn_2O_4$ electrode was prepared. The discharge capacity of the produced $LiMn_2O_4$/MWCNT nanocomposite electrode was cyclically tested, and the charge transfer resistance of the electrodes was studied using electrochemical impedance spectroscopy. Consequently, the Au–Pd-coated $LiMn_2O_4$/MWCNT had a 120 mAh g^{-1} discharge capacity and 90 % capacity retention after 100 cycles.

Keywords $LiMn_2O_4$/MWCNT · Flexible electrode · Composites · Electrochemical performance

1 Introduction

Recently, researchers have attempted to produce flexible electrodes because soft, bendable, and porous electrodes may be used in flexible lithium ion batteries, which in turn could be utilized in displays that can be rolled up, in smart electronics, in wearable devices and in other applications. Many studies regarding flexible electrodes utilized CNT or graphene [1–3]. The major classes of cathode materials currently used for lithium ion batteries, such as $LiCoO_2$, lithium manganese oxide ($LiMn_2O_4$) and $LiFePO_4$, are generally synthesized using high-temperature processes. However, fabricating flexible cathodes remains difficult because most flexible substrates or their precursors are unstable at high temperatures [4, 5].

Among the commonly used cathode materials, $LiMn_2O_4$, which has a cubic spinel structure, is a promising cathode material for rechargeable lithium ion batteries because it has advantages such as a lower cost, the high abundance of manganese (Mn) in the earth, a good safety profile, and low toxicity. However, the spinel $LiMn_2O_4$ irreversibly loses capacity while cycling. After comprehensively investigating the mechanism for the capacity decreases in the spinel $LiMn_2O_4$ positive electrode, several factors, including Mn dissolution, electrolyte decomposition, structural instability during charge–discharge cycling, Jahn–Teller distortion, and the transforming crystallinity, were proposed to be responsible for the losses in capacity [6–10]. Moreover, increasing the electrical conductivity of and forming a networked structure with $LiMn_2O_4$ supported on multi-wall carbon nanotubes (MWCNTs) with a large surface area might be an ideal method for functionalizing the active material in preparation for its use in energy conversion and storage [11]. Therefore, hybrid nanostructures composed of MWCNTs and active materials should possess not only the inherent properties of the nanocrystals and MWCNTs acting separately but also the additional, unique properties arising from their electrical and thermal interactions [12].

T. Cetinkaya (✉) · M. O. Guler · H. Akbulut
Department of Metallurgical & Materials Engineering, Engineering Faculty, Sakarya University, Esentepe Campus, 54187 Sakarya, Turkey
e-mail: tcetinkaya@sakarya.edu.tr

A. Akbulut
Department of Environmental Engineering, Engineering Faculty, Sakarya University, Esentepe Campus, 54187 Sakarya, Turkey

In this work, we sought to increase both the specific capacity and the stability of the $LiMn_2O_4$ spinel cathode material. To overcome the difficulties caused by $LiMn_2O_4$, we pursued a hybrid $LiMn_2O_4$/MWCNT nanocomposite as a flexible cathode material with a highly porous structure originating from the MWCNT network. Although there has been an enormous number of carbon-supported nanocomposite $LiMn_2O_4$ cathodes published to date, our work is the first to impregnate the $LiMn_2O_4$ active material into MWCNT buckypaper by coating the surfaces of the nanotubes. Consequently, $LiMn_2O_4$ cathode material was first produced using a facile sol–gel method. To prepare the electrode, a $LiMn_2O_4$ slurry was prepared to coat the previously prepared flexible carbon nanotube buckypapers. Furthermore, the surfaces of the produced electrodes were coated with a gold–palladium (Au–Pd) alloy, thus providing a thin interphase layer between the electrolyte and electrode to prevent Mn dissolution during the charge/discharge process.

2 Experimental procedure

2.1 Preparation of $LiMn_2O_4$

The $LiMn_2O_4$ powders were produced using a well-known sol–gel method at a low temperature to obtain very fine nanocrystalline structures. Manganese acetate tetrahydrate ($Mn(CH_3COO)_2{\cdot}4H_2O$), lithium acetate dehydrate ($LiCH_3COO{\cdot}2H_2O$), and citric acid were used during the process. First, $Mn(CH_3COO)_2{\cdot}4H_2O$ (99.999 %, Sigma-Aldrich) was dissolved in 50 ml distilled water. $LiCH_3COO{\cdot}2H_2O$ (99.999 %, Sigma-Aldrich) was subsequently added with gentle stirring; citric acid was added to this solution as a chelating agent, and ammonia was introduced to maintain the pH between 7 and 10. Afterward, the solution was heated with vigorous stirring to remove any excess ammonia or water. The temperature was gradually increased from 60 to 90 °C with continued vigorous stirring until a transparent gel was obtained. The resultant gel was dried at 120 °C for 10 h before being calcined at 300 °C for 24 h in air.

2.2 Preparation of flexible MWCNT paper

MWCNT (purity 95 %, diameter 50–100 nm) was purchased from Arry Nano Materials, and MWCNT paper was produced using a vacuum filtration technique. Before the vacuum filtration technique was enacted, the MWCNTs were purified and functionalized. To purify the MWCNTs, a specific amount of MWCNT was baked at 350 °C for 1 h before a 1 h treatment with hydrochloric acid (HCl) to remove the amorphous carbon and some impurities. After the chemical treatment, the MWCNTs were washed with water several times until a pH between 6 and 7 was reached. After the purification process, the MWCNTs were functionalized in sulfuric acid/nitric acid (3/1) for 2 h with magnetic stirring at room temperature. They were subsequently filtered, washed with water until the rinses had a neutral pH and dried in a 40 °C oven for 24 h. Next, 40 mg of the purified and functionalized MWCNTs was added to 50 ml pure water and dispersed with an ultrasonic homogenizer; the MWCNT suspensions were vacuum filtered to form the MWCNT paper. The MWCNT film was peeled from the PVDF membrane to obtain the flexible MWCNT paper. The produced MWCNT paper was approximately 100 μm thick.

2.3 Preparation of the electrodes

To prepare the flexible electrodes, a slurry was prepared that contained 75 wt %. $LiMn_2O_4$ powder, 10 wt %. acetylene black, and 15 wt % PVDF binder dissolved in 10 ml *N*-methyl-2-pyrolidone (NMP). The slurry was cast on the prepared MWCNT paper and kept in a fume hood for 24 h to absorb the slurry and disperse the $LiMn_2O_4$ powders within the porous structure of the MWCNT paper; consequently, the MWCNT surface was coated with active $LiMn_2O_4$. During the last step, the $LiMn_2O_4$-coated MWCNT paper electrodes were dried in a 120 °C oven for 24 h and were then cut using a cutter disc to a size suitable for assembling the CR2016 test cell. To compare the effect of our nanocomposite structure on the cell's electrochemical performances, a bare $LiMn_2O_4$ electrode was formed on aluminum foil (thickness of 200 μm) using same slurry as described above. Furthermore, the surfaces of the $LiMn_2O_4$/MWCNT composite and the bare $LiMn_2O_4$ electrodes were coated with a Au–Pd alloy via magnetron sputtering to obtain a thin ($\sim$10 nm) and a conductive layer between the electrolyte and electrode to prevent Mn dissolution.

2.4 Physical and electrochemical characterization

The phase and structural analyses of the nanocomposites were conducted via powder X-ray diffraction (XRD) using a Rigaku D/MAX 2000 X-ray generator and diffractometer with Cu Kα radiation. The diffraction patterns were collected in step scan mode and recorded in 1° (2θ) steps at 1 min per step when $10° < 2\theta < 90°$. Scanning electron microscopy (SEM) (Jeol 6060LV) was used to investigate the microstructure of the nanocomposite electrodes.

The electrochemical performance and charge–discharge profiles of the electrodes were assessed from 3.0 to 4.3 V at a constant rate of 1C. The specific capacities of the produced electrodes were calculated based upon the $LiMn_2O_4$ weight. Electrochemical impedance spectroscopy (EIS) measurements were performed on the samples after 10

cycles with a Gamry Instrument Version 5.67, using a sine wave with a 10 mV amplitude over a frequency range of 1,000 kHz–0.1 Hz to compare composite electrode's charge transfer resistance with bare $LiMn_2O_4$ electrode's charge transfer resistance and to investigate the effect of the Au–Pd coating on the electrodes.

3 Results and discussion

3.1 Characterization of the composite structure

The preparation of the buckypapers and $LiMn_2O_4$/MWCNT flexible cathodes are depicted in Fig. 1. Figure 1a shows a schematic view of the filtration method used to produce the flexible MWCNT papers. Figure 1b and c display the surface of the $LiMn_2O_4$ powder-coated MWCNT papers after a scalpel was used to remove the composite electrodes from the CR2016 test cell assembly. The $LiMn_2O_4$/MWCNT nanocomposite remained flexible after the coating process and even after drying at 120 °C.

XRD patterns for the MWCNT paper, bare $LiMn_2O_4$ powder, and $LiMn_2O_4$/MWCNT nanocomposite are presented in Fig. 2. For the MWCNT paper, the (002) and (101) planes provide the carbon peaks observed at 2θ values of 26.3° and 44.4°, the reflection peaks and planes of the MWCNT paper validate work of Yue et al. [13]. Moreover, the typical reflection peaks for $LiMn_2O_4$ at 2θ values of 18.56°, 36.12°, 37.6°, 44.02°, 48.06°, 58.03°, 63.98°, and 67.42° represented the (111), (311), (222), (400), (331), (511), (440), and (531) planes, respectively, for the spinel structure in $LiMn_2O_4$ [14]. After preparation of the $LiMn_2O_4$/MWCNT composite electrode, it is interesting to note that new reflection peak was observed at 2θ values of 34°. It should be due to existence of the PVDF binder and acetylene black in the composite electrode.

Figure 3 shows the surface morphology of the $LiMn_2O_4$ powders and a cross-sectional image of a $LiMn_2O_4$/MWCNT composite electrode. A low-magnification SEM image depicting bare $LiMn_2O_4$ powders is presented in Fig. 3a, revealing that $LiMn_2O_4$ has a porous structure after calcination at 300 °C for 24 h. A high-magnification SEM

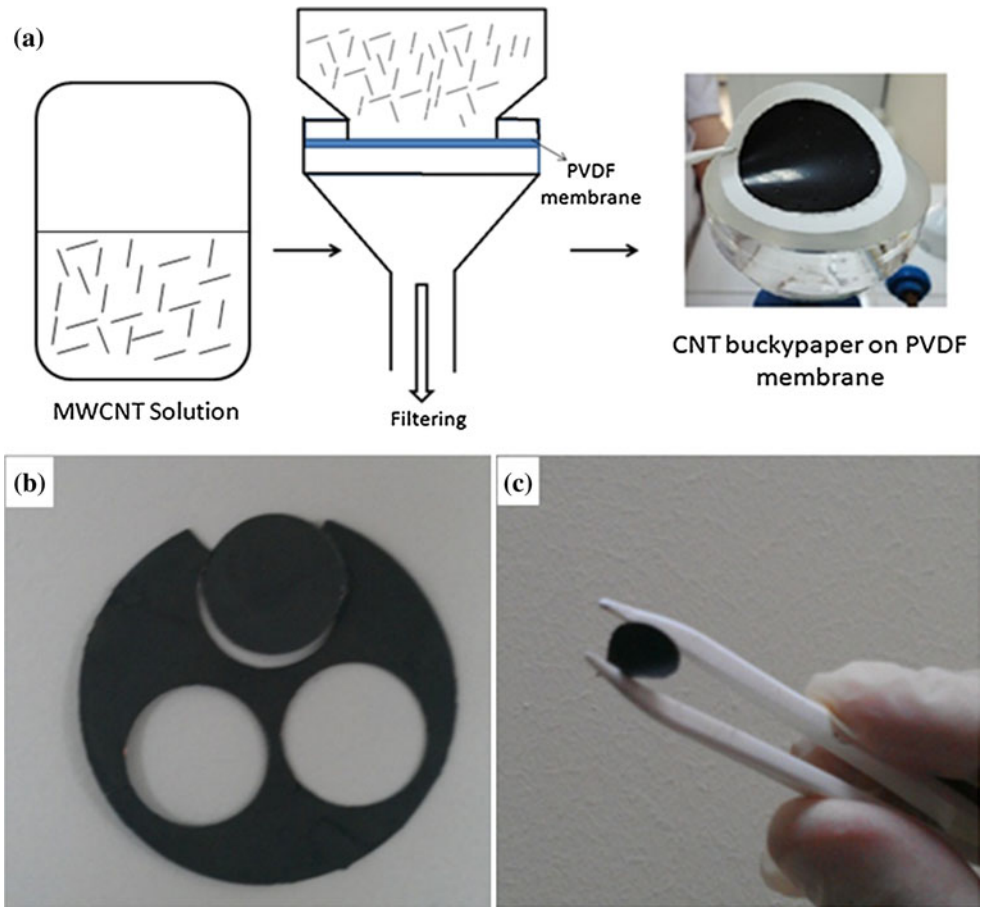

Fig. 1 **a** Schematic of the vacuum filtration method used to produce the MWCNT papers, **b** $LiMn_2O_4$/MWCNT composite electrode after cutting, and **c** flexibility of the $LiMn_2O_4$/MWCNT nanocomposite demonstrated with tweezers

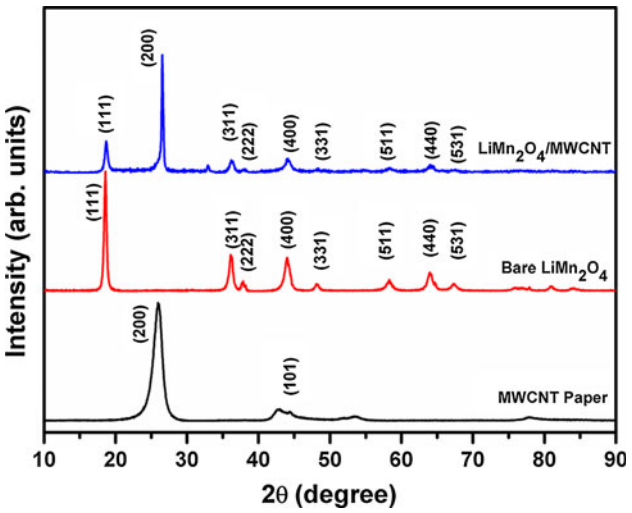

Fig. 2 XRD patterns of the MWCNT paper, bare $LiMn_2O_4$ powders, and $LiMn_2O_4$/MWCNT nanocomposite electrode

image of the $LiMn_2O_4$ powders clearly indicates that the structure of the $LiMn_2O_4$ powders included nanoscale $LiMn_2O_4$ grains (Fig. 3b). This $LiMn_2O_4$ structure allows lithium ions diffuse, facilitating the reactions between the lithium ions and active materials [15]. Figure 3c, d shows high- and low-magnification SEM images of the $LiMn_2O_4$/MWCNT composite electrode. Figure 3c indicates that the bottom side of the electrode is MWCNT paper, while the top side of the electrode includes the $LiMn_2O_4$ powders that were applied using a scalpel. The high-magnification image of the bottom of the $LiMn_2O_4$/MWCNT electrode demonstrates that the nano $LiMn_2O_4$ powders were embedded in the CNT interspaces.

3.2 Electrochemical characterization of the composite

The charge–discharge curves of bare $LiMn_2O_4$ and $LiMn_2O_4$/MWCNT composite electrodes are displayed in Fig. 4. Figure 4a and b clearly indicate that the electrode's curve reveals two plateaus at approximately 4.0 V during the charge/discharge process; this profile is typical for the electrochemical insertion and extraction of lithium ions into and from a $LiMn_2O_4$ electrode [12]. As presented in Fig. 4a and b, the $LiMn_2O_4$/MWCNT nanocomposite electrode had a significantly improved specific capacity relative to the bare, porous $LiMn_2O_4$. This performance enhancement is attributed to the nanocomposite electrode's improved electrochemical accessibility and a decrease in the inert "dead" zones caused by the interpenetrating conductive MWCNT networks present in the composite structure. In Fig. 4a and b, the $LiMn_2O_4$/MWCNT nanocomposite electrode displayed not only a higher initial

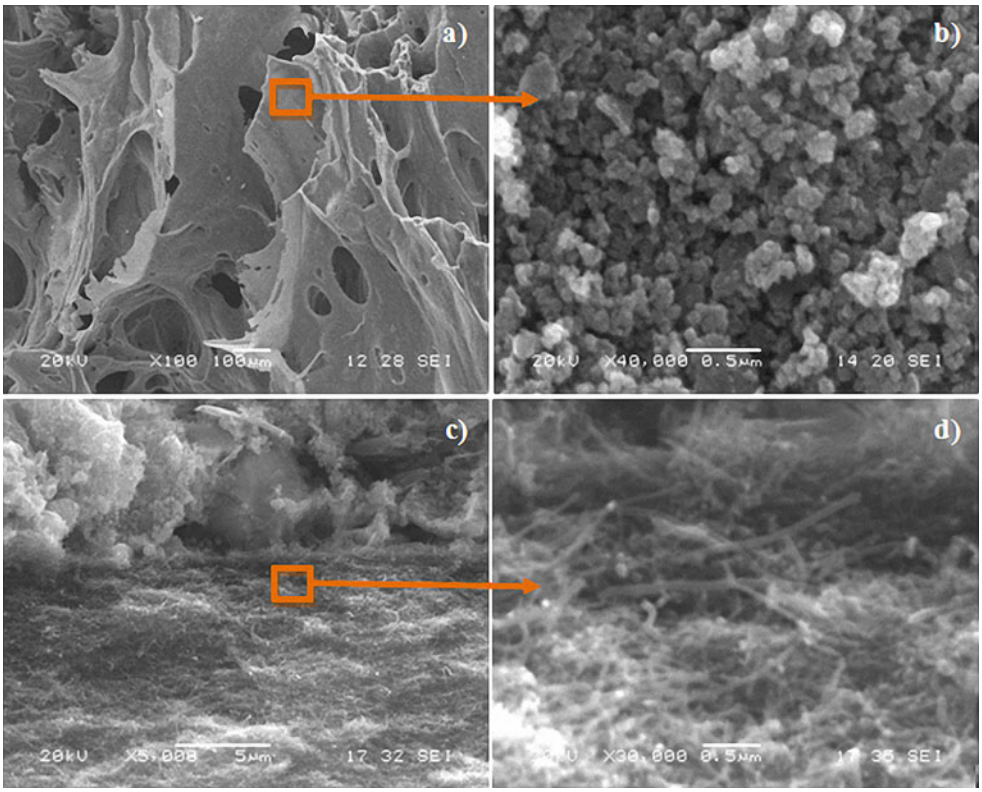

Fig. 3 Low- and high-magnification SEM images of **a**, **b** bare $LiMn_2O_4$ and **c**, **d** $LiMn_2O_4$/MWCNT nanocomposite, respectively

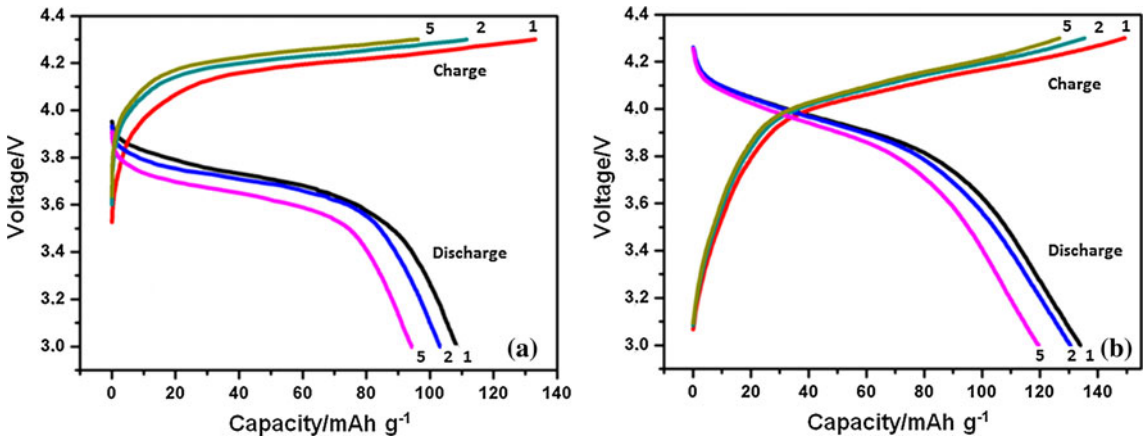

Fig. 4 Charge–discharge curves of **a** bare-$LiMn_2O_4$ and **b** $LiMn_2O_4$/MWCNT composite

capacity, but also a greater enlargement of the charge–discharge curves relative to the bare $LiMn_2O_4$ electrode. The high hysteresis between the charge–discharge curves in the nanocomposite electrodes involved the Li insertion and removal. The mechanisms were detailed by Wang et al. [16] and Li et al. [17]. These groups reported that the enlarged curves revealed the higher electrode reactivity with lithium ions because increasing the lithium ions' reaction with the electrode depended on the electrode's conductivity. These reports indicate that our composite structure leads to increases in the lithium ion reaction and higher initial discharge capacity. Therefore, our composite structure might provide efficient electronic transport throughout the cathode and helpfully decrease the electrode's resistivity.

To investigate the charge transfer resistance of the bare $LiMn_2O_4$, the $LiMn_2O_4$/MWCNT nanocomposite and their respective Au–Pd-coated electrodes, the EIS of the produced electrodes were measured after 10 cycles and are presented in Fig. 5. The EIS spectra of the produced electrodes were well fitted on an equivalent circuit. On this circuit, R_s is the electrolyte's resistance, R_{int} is the resistance of any film formed on the cathode surface (first HF semicircle), R_{ct} is the charge transfer resistance of the electrode's reaction with lithium ions (middle frequency semicircle), and W_{dif} is the resistance of the lithium ion diffusion to the electrode (low frequency semi-circle) [18]. The R_{ct} of the electrodes was investigated after fitting the samples to the equivalent circuit; the charge transfer resistance of the bare $LiMn_2O_4$ was 566 Ω. However, the charge transfer resistance of the $LiMn_2O_4$/MWCNT composite electrode was 100.5 Ω; this value was somewhat lower than the charge transfer resistance of the bare $LiMn_2O_4$ electrode. Therefore, the MWCNTs increased the reactivity of the lithium ion toward electrode because the CNT structures are highly conductive. Furthermore, the

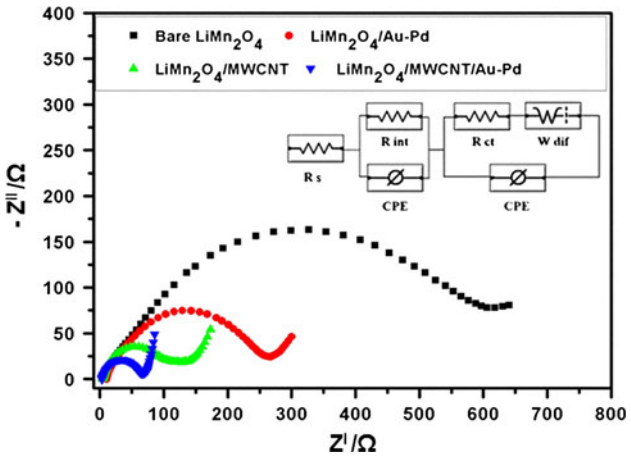

Fig. 5 EIS spectra of the produced electrodes and an equivalent circuit

charge transfer resistance of the Au–Pd-coated $LiMn_2O_4$/MWCNT was 60.84 Ω, giving this system the lowest charge transfer resistance among the produced electrodes. The Au–Pd-coated $LiMn_2O_4$/MWCNT has the lowest charge transfer resistance most likely because the Au–Pd thin film prevents Mn from dissolving in the electrolyte. However, the bare $LiMn_2O_4$ electrode's capacity faded rapidly because the Mn dissolved in the electrolyte, leading to an increased charge transfer resistance in the electrode. The gold nano-layer might reduce the contact area at $LiMn_2O_4$ electrode/electrolyte interface and therefore hinder the dissolution of Mn and the oxidation of the electrolyte, as reported by Tu et al. [19].

Figure 6 shows the discharge capacities as a function of the charge/discharge cycles for the bare $LiMn_2O_4$, $LiMn_2O_4$/MWCNT composite and their respective Au–Pd-coated electrodes at room temperature. The bare $LiMn_2O_4$ had a high initial capacity (108 mAh g^{-1}), but the cell performance decreased sharply as the cycle number

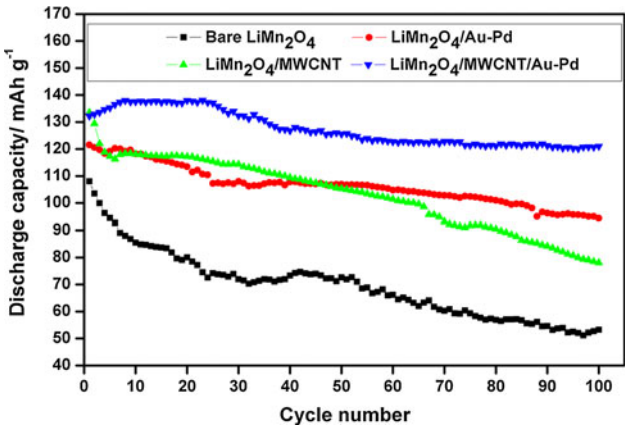

Fig. 6 Electrochemical cyclic tests on produced electrodes

increased. However, the $LiMn_2O_4$/MWCNT composite electrode demonstrated a higher initial discharge capacity and better capacity retention when the cycle number increased. The Au–Pd-coated composite electrode retained its capacity after 40 cycles, and a 90 % capacity retention was obtained for the surface-coated composite electrode after 100 cycles. The $LiMn_2O_4$/MWCNT/Au–Pd composite electrode retained its capacity most likely because the highly conductive structure of the CNT and the thin layer of Au–Pd. CNT increase the cathode's reaction with lithium ions due to the conductive structure of the CNT, while the thin Au–Pd layer prevents Mn dissolution in the electrolyte.

4 Conclusion

Flexible $LiMn_2O_4$/MWCNT composite electrodes were successfully produced. Our composite structure greatly improved the electrochemical performance of a bare $LiMn_2O_4$ cathode using the highly conductive structure of CNT; applying Au–Pd coatings to the surface of nanocomposite electrodes improves their cyclability and capacity retention. The $LiMn_2O_4$/MWCNT nanocomposite electrodes displayed a significantly improved specific capacity due to their interpenetrating conductive MWCNT networks. Au–Pd-coated flexible $LiMn_2O_4$/MWCNT cathodes exhibit a 120 mAh g^{-1} discharge capacity, even after 100 cycles. In addition, the charge transfer resistance of the nanocomposite electrodes was significantly decreased. Because the $LiMn_2O_4$/MWCNT nanocomposite electrodes are naturally flexible, we envision that these nanocomposite electrodes might be developed as next generation positive electrodes for high power Li-ion batteries.

Acknowledgments This work is supported by the Scientific and Technological Research Council of Turkey (TUBITAK) under the contract number 111M021. The authors thank the TUBITAK MAG workers for their financial support.

References

1. Chew SY, Ng SH, Wang J, Novak P, Krumeich P, Chou SL, Chen J, Liu HK (2009) Carbon 47:2976–2983
2. Wang JZ, Zhong C, Chou SL, Liu HK (2010) Electrochem Commun 12:1467–1470
3. Chou SL, Wang JZ, Chew SY, Liu HK, Dou SX (2008) Electrochem Commun 10:1724–1727
4. Jia X, Yan C, Chen Z, Wang R, Zhang Q, Guo L, Wei F, Lu Y (2011) Chem Commun 47:9669–9671
5. Zhou W-J, He B-L, Li H-L (2008) Mater Res Bull 43:2285–2294
6. He BL, Zhou WJ, Liang YY, Bao SJ, Li HL (2006) J Colloid Inteface Sci 300:633–639
7. Tu J, Zhao XB, Cao GS, Tu TP, Zhu TJ (2006) Mater Lett 60:3251–3254
8. Ye SH, Lv JY, Gao XP, Wu F, Song DY (2004) Electrochim Acta 49:1623–1628
9. Liu H, Cheng C, Zongqiuhu, Zhang K (2007) Mater Chem Phys 101:276–279
10. Thirunakaran R, Sivashanmugam A, Gopukumar S, Dunnill CW, Gregory DH (2008) Mater Res Bull 43:2119–2129
11. Bülow JF, Zhang HL, Morse DE (2012) Adv. Energy Mater 2:309–315
12. Liu XM, Huang ZD, Oh Z, Ma PC, Chan PCH, Vedam GK, Kang K, Kim JK (2010) J Power Sources 195:4290–4296
13. Yue L, Zhong H, Zhang L (2012) Electrochim Acta 76:326–332
14. Zhao X, Hayner CM, Kung HH (2011) J Mater Chem 21:17297
15. Shaju KM, Bruce PG (2008) Chem Mater 20:5557–5562
16. Wang L, Huang Y, Jiang R, Jia D (2007) J Electrochem Soc 154:A1015–A1019
17. Li X, Kang F, Shen W (2006) Carbon 44:1298–1352
18. Yang S, Huo J, Song H, Chen X (2008) Electrochim Acta 53:2238–2244
19. Tu J, Zhao XB, Cao GS, Tu JP, Zhu TJ (2006) Mater Lett 60:3251–3254